Honeycomb-Inspired Metamaterial for Tactile Sensors with Variable Stiffness

Rustam Chibar, Valeriya Kostyukova, Soibkhon Khajikhanov, Daryn Kenzhebek, Altay Zhakatayev, Bakhtiyar Orazbayev, Zhanat Kappassov

Honeycomb-Inspired Metamaterial for Tactile Sensors with Variable Stiffness

Rustam Chibar, Valeriya Kostyukova, Soibkhon Khajikhanov, Daryn Kenzhebek, Altay Zhakatayev, Bakhtiyar Orazbayev, and Zhanat Kappassov, *Senior Member, IEEE*

***Abstract*— The material's stiffness plays a crucial role in tactile sensors and stiffness controllers of robot joints, enabling robots to interact with the environment. Conventional controllers or sensors require apriori information about stiffness modulation to efficiently control the collision with the environment and reduce its detrimental effects. Therefore, such inflexibility of real-time stiffness variation may cause instability if the dynamic mechanical system (a mass-spring-damper) changes during execution. In this paper, we tackle the problem using a honeycomb metamaterial with a tunable stiffness to design a tactile sensor capable of detecting physical contact with low and high-impact forces. We experimentally demonstrate that dynamic modification of the honeycomb structure reduces the maximum impact force by $\approx 30\%$, mitigating the rapid collision with the environment during contact detection. The results show that the honeycomb attachment allows for a more precise and controlled impact with varying degrees of energy and momentum transfer. The honeycomb attachment can be a valuable tool for grasping, explosive motion generation, and tactile sensing, requiring low-or-high-impact and controllable contact. Our study highlights the potential of using negative stiffness honeycomb structures to improve the functionality of tactile sensors.**

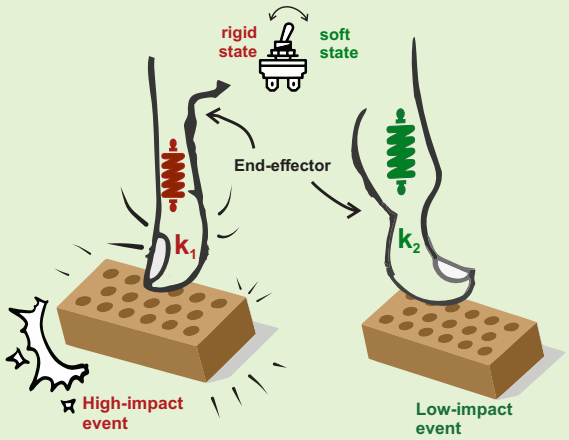

***Index Terms*— Force and tactile sensing, collision detection, compliance and impedance control, variable stiffness, tactile sensors, physical inte ractions, nonlinear stiffness, honeycombs, potential energy storage.**

I. INTRODUCTION

As the integration of robots into logistics, manufacturing, healthcare, and service continues to increase, the possibility of physical interaction between a human and a robot also grows. This, in turn, puts an increased demand for safety, adaptability to the environment, and autonomous performance capabilities of robots. A robot is considered safe if it does not harm a human, itself, or the environment during its operation and interaction with humans. A robot must be compliant during disturbances and remain safe in nominal conditions, unforeseen circumstances, and unpredictable conditions [1].

The safety of a robot manipulator necessitates the accurate detection of collisions and the appropriate reaction to them [2]. There are two main concepts for collision detection: model-based and sensor-based. The model-based method is an arduous task. It requires torque sensors at every joint of the robot and computation of its corresponding inertia matrix at every time instance to estimate the external torques based on the dynamic equations. However, the exact values of dynamic model parameters (such as motor inertia or damping coefficient) are often not available, while experimentally estimating them might require complex, time, and resource-consuming experiments [3]. The robot model with approximate parameter values results in a high variation and uncertainty in the torque threshold level for contact detection, thus decreasing safety.

On the other hand, sensor-based methods could be deployed on simpler yet reliable position-controlled robots. Such an approach does not require formulating an accurate dynamic model of the robot and environment [4]. The contact is detected by only analyzing the data from tactile sensors. However, these sensors are usually noisy and potentially dangerous since a small error in sensor readings may lead to high-impact forces during collisions, especially if the sensing layer is thin and rigid.

Soft tactile sensors are one way to simplify the system and guarantee a safe physical human-robot interaction. These soft sensors can detect collisions, dampen their impact forces, and control the momentum transfer during the interactions [5]. However, the significant downsides of soft tactile sensors

Submitted March 2024 and revised month year.
Corresponding author: B. Orazbayev.
RC is with the Institute of Smart Systems and Artificial Intelligence, Nazarbayev University, Astana, Kazakhstan.
VK, SK, DK and ZK are with the Department of Robotics Engineering, School of Engineering and Digital Sciences, Nazarbayev University, Astana, Kazakhstan. Corresponding author: Z. Kappassov, email: zhkappassov@nu.edu.kz.
AZ is with Mechanical and Aerospace Engineering Department, Nazarbayev University, Astana, Kazakhstan.
BO is with Physics Department, Nazarbayev University, Astana, Kazakhstan.
This work was funded by MSHE Kazakhstan Grant number AP23485307 or AP23485994, by Nazarbayev University under FD-CRGP no. 11022021FD2923, 11022021FD2901 and 201223FD2606.

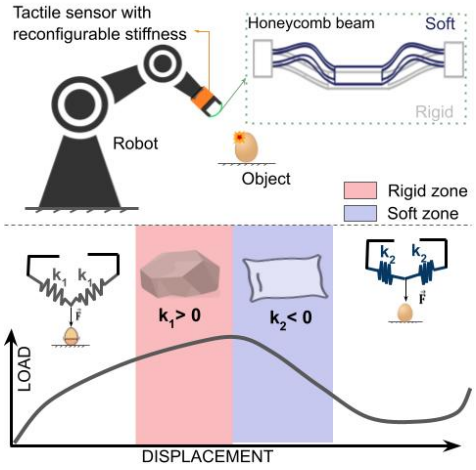

Fig. 1: Tunable stiffness honeycomb-inspired soft tactile sensor attached as an end-effector to a robot interacts with a fragile object. The honeycomb-based metamaterial (right inset), has a non-linear force-displacement characteristic with rigid and soft states (red and blue areas in the bottom plot) and variable stiffness behavior. Adjusting the honeycomb beam's buckling displacement allows the stiffness to be tuned from a rigid (left inset) to a soft (right inset) state.

are their limited sensitivity, responsiveness, and bandwidth compared to rigid-material-based sensors [6]. Multiple attempts have been made to improve the sensing performance of soft sensors [7]. Fortunately, we can circumvent these difficulties by utilizing hybrid sensors (incorporating rigid-soft designs) [8], or tactile sensors with variable stiffness (hard-soft states) [9] that can modify the system's resonance frequency and ensure the stability of the physical interaction while providing a better frequency bandwidth and sensitivity. While the hybrid sensors can reduce the impact forces, switching between hard and soft states allows changing the sensor properties on-the-fly before or during collisions, which is crucial for avoiding resonance instability [10], [11].

A promising approach for designing soft tactile sensors is to employ metamaterials – artificially engineered structures that exhibit unique mechanical properties not found in natural materials owing to their specific geometric configurations. For instance, such structures may possess unusual properties: variable stiffness (positive and negative) [12], auxetic behavior [13] or negative Poisson's ratio [14], and visco-elastic behavior [15]. The auxetic structure is applied in protective equipment and fabrics [16]. Another example, origami-inspired structures, popular in space applications and soft robotics, can also be considered mechanical metamaterials since their folding patterns give several valuable properties, such as programmable stiffness, anisotropic elasticity, and energy absorption [17]. Finally, negative stiffness can be achieved and designed using the curved beams or von Mises trusses [13]. In Von Mises trusses, the load can pass through zero displacement, called snap-through behavior. They are popular in morphing applications because they have bi-stable properties due to the symmetric design [18]. Bi-stability is also popular in MEMS as a mechanical state switch since it remains in one of its states without the constant external force [19], [20]. In contrast, a metastable structure has one stable and one quasi-stable state. Such metastable structures always return to their stable state without external forces. In our study, we implement a metastable structure with curved beams as the variable stiffness elements to achieve tunable stiffness.

Therefore, in this work, we propose using metamaterial structures composed of negative stiffness honeycomb beams to design and construct a soft tactile sensor with an active surface. To our knowledge, this is the first time mechanical metamaterial is used as an active end-effector for robot manipulators. We experimentally demonstrate the superior performance of the metamaterial structure in applications for contact detection, stiffness variation, and energy storage. We perform the following experiments to assess the feasibility of the metamaterial structure: contact detection and impact response variation based on stiffness adjustment. The contact detection experiment is designed to evaluate the sensitivity of the honeycomb structure in responding to contact forces under different pre-compression levels. The impact response variation based on stiffness adjustment experiments examines the structure's ability to store and release the potential energy during high-impact events, providing the solution for both safe interaction and maximizing the impact by providing extra momentum.

The structure of the paper is as follows: we start by reviewing existing works on collision detection methods, sensor-based contact sensing, and mechanical metamaterials in Section II. This is followed by a brief description of the theory describing the honeycomb behavior and design in Section III. Then, in Section IV, we report our design of an end-effector based on a metamaterial structure consisting of negative stiffness honeycombs for a robot arm (Fig. 1). We test the proposed metamaterial in two experiments and analyze the obtained results in Section V. Finally, we summarize the beneficial properties of the proposed metamaterial structure in Section VII.

II. Related work

A. Robot collision detection and contact sensing

The common framework to deal with the collision is based on the collision event pipeline [21], where collision detection with the environment is the first phase in the mentioned pipeline. Below, we review three main approaches used for collision detection.

1) Model-based collision detection methods: In this method, a model of a system, together with the output, state, and input signals, are used to estimate the dynamic forces and torques. The disturbance observers are used to identify the unknown states and parameters of the robot's dynamic system and to detect possible collisions. The main sensors used in the model-based approach are motor current sensors and joint encoders [21]–[24]. Researchers provide various model-based collision detection algorithms for arm manipulators and legged robots based on momentum observer [2]. The main idea of the momentum observer is monitoring the estimated external torques exerted on the robot and comparing them with actual torques applied on joints. Mamedov et al. [25] showed that the momentum observer is both flexible and simple for tuning and requires the least time to predict the collision compared

to other types of observers such as sliding mode observer [23], nonlinear disturbance observer [26], Kalman disturbance observer [27], and filtered dynamics [28]. The momentum observer is successful and cost-effective in detecting collisions, as it estimates the sum of all torques generated by the collision, but in perfect conditions. Van et al. [29] provided a model-based collision detection and identification basis for a quadrupedal robot with unmodeled loads. They utilized the band-pass filtered external forces and chosen threshold level to detect the collision by estimating the time span. Cao et al. [30] proposed a model-based collision detection with sequential dynamics identification and state-dependent dynamic threshold based on the Lasso regression analysis method. Selecting the values for static and dynamic parameters for model-based collision detection algorithms is very challenging and may not be applicable to all manipulators.

2) Sensor-based contact sensing: The sensor-based method is a statistical method that relies on the sensor data only. To understand the nature of contact, get feedback, and utilize it for further interaction with the environment, tactile sensors are integrated into the robotic system. Dahiya et al. [31] reviewed the classification of robotic tactile sensing and classified sensor types according to their working physical principle (resistive, capacitive, optical, ultrasonic, magnetic, piezoelectric sensors) and physical properties (gels, conductive rubber, etc.). Some authors use a combination of sensors to get a multi-modal tactile sensing system. Patel et al. [32] showed a dynamic tactile sensor based on pressure, contact, and force sensor embedded in a soft polymer. Mittendorfer et al. [33] presented a relatively tiny multi-modal tactile-sensing module consisting of acceleration, temperature, and proximity sensors emulating human skin. The material structure of an object can be recognized by analyzing the vibrations during the contact between a tactile sensor and the object as done by [34]. Kaboli et al. [35] presented the descriptors for differentiating textures and objects via robot skin based on multimodal tactile sensors that consist of an accelerometer, proximity sensor, normal-force sensor, and temperature sensor.

3) Data-driven collision detection methods: Machine learning-based methods can be viewed as a mix of the aforementioned two methods. They use the robot dynamic model coupled with data from joint torque or current sensors to detect collisions [36]. These methods are robust with respect to model uncertainties, parameter variations, and sensor noise. Sharkawy et al. [37] provided a multilayer feedforward neural network, where joint positions, velocities, torques, and other variables are taken as the input, while the estimated external torques are the output. Park et al. [36] presented 1-D CNN and support vector machine regression, coupled with momentum observers, as the main approach to detect hard and soft collisions. However, they needed to collect data for three different scenarios: hard collisions, soft collisions, and collision-free motion. In their recent work [38], authors provided a collision detection method using an unsupervised anomaly detection algorithm by autoencoders requiring only motor current measurement and basic robot dynamics model without friction term. Kim et al. [39] provided a modularized neural network by leveraging the dynamics decoupling for each manipulator joint and transfer learning for mass production. However, one common disadvantage of these data-driven methods is that they require large datasets of free from collisions joint torques in the target robot.

While the above-mentioned studies focus on either a passive or active approach to sensing, in the next paragraph, we aim to show the dual-functionality (sensing and actuation) of metamaterial structure, highlighting its potential utilization for diverse applications.

B. Metamaterials

Mechanical metamaterial structures, based on their design and geometry, can be divided into honeycombs, origami-inspired structures, shape memory effect (SME) structures [13]. There are two types of honeycomb structures: hexagonal honeycombs and negative stiffness honeycombs (NSH) [15]. The hexagonal honeycomb structure has a property of negative Poisson's ratio which is beneficial for the structure since it provides enhanced stiffness, flexibility, and energy absorption [14]. However, one of the main disadvantages of the hexagonal honeycomb structure is its unrecoverability, which means that the compressed hexagonal structure can not be restored to its initial shape due to plastic deformation. In other words, the hexagonal honeycomb structures are for one-time use only. The NSH is formed by several curved clamped-clamped beams arranged in parallel and in series. A systematic and deep understanding of the quasi-static and dynamic loading behaviors of the NSH is crucial to their practical applications. Many papers describe the behavior of different types of NSHs on quasi-static and dynamic tests. Chen et al. [40] conducted quasi-static compression for investigating mechanical performances, cyclic experiments for exploring reusability, vibration isolation tests for discovering vibration control effects, and plate-impact experiments for studying cushion properties. These tests are conducted because geometric parameters could have a great influence on the mechanical behavior of the metamaterial structure i.e. limit in force, buckling, and bi-stability. The use of NSH allows absorbing the impact energy without transmitting it to an insulated object as opposed to conventional springs with linear stiffness [15], [41], [42]. Some authors introduced the NSH structure as a 2D/3D construction and provided a numerical analysis through quasi-static and dynamic tests [43], [44]. Mechanical programming is another direction in which mechanical metamaterials have great potential. As one of the properties of metamaterial is bi-stable reconfigurability, it can be used as reprogrammable mechanological metamaterial (ReMM) for combinatorial and sequential logic such as NAND [20], AND, OR, and NOT logic gates [45]. Additionally, mechanical metamaterials can be designed to exhibit a temperature-dependent shape memory effect such that changes in temperature result in flexible shape-changing capabilities, including multistable reconfigurations, stimulus-activated restoration, and energy absorption during compression [46]. Our focus is on investigating the dynamic properties of the clamped-clamped double-curved NSH beams. A brief presentation of the theoretical background and a

detailed description of the design is presented in the following sections.

III. Theoretical Background

A. Curved beam design

Consider a clamped-clamped cosine-shaped double-curved beam in Fig. 2a, where $w(x)$ - the transverse curve of the beam. The curve is taken from the first buckling mode, which is shown in [47], and, mathematically, is obtained by the equation

$$w(x) = \frac{h}{2}[1 - \cos(2\pi \frac{x}{L})]. \tag{1}$$

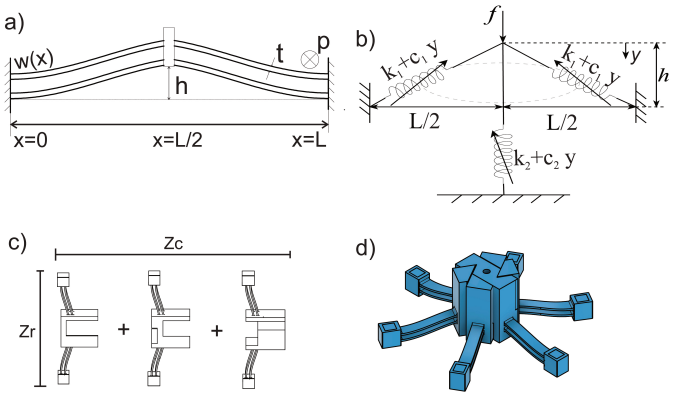

Fig. 2: Negative Stiffness Honeycomb metamaterial design: a) schematic drawing of the double curved beam with geometric and shape parameters; b) schematic illustration of honeycomb beam model with two springs k_1 and one spring k_2; c) three NSH parts, each has one double beam of the honeycomb; d) assembled NSH for the tactile sensor.

Let the Young's modulus of the material be denoted as E, the horizontal length of beam as L, depth of beam p, number of rows of beam Z_r, number of columns of beam Z_c, force of local maximum f_{max}, force of local minimum f_{min} such that $0 < |f_{min}| < |f_{max}|$. These parameters are the necessary inputs for Algorithm 1 in Zhakatayev et al. [12], which outputs the thickness of each beam t and apex height (height of the middle point of the beam) h. These parameters are important for designing the metastable, critically stable, or bistable honeycomb structures [12], [47].

As mentioned before, the concept of variable stiffness behavior might involve both positive and negative stiffness phases. The schematic illustration of the mechanical system that models the behavior of the honeycomb is shown in Fig. 2(b). This system can produce nonlinear stiffness behavior, generating negative stiffness by oblique springs and positive stiffness by a vertical spring. Theoretically, it is impossible to create a monostable system with only oblique springs, because, in that case, the system will rapidly cross zero-level displacement (snap-through behavior) and will go to the second equilibrium position with mechanical energy stored during initial deformation. In our proposed design of the honeycomb, one double-curved beam is represented by two oblique springs in the mechanical model. Material defects, rough surfaces, and other imperfections introduced during the manufacturing process lead to variations in the parameters of the beam, which in turn implies that each of the honeycomb beams has slightly different stiffness characteristics. For their nonlinear force-displacement properties, the springs in Fig. 2b are denoted to be nonlinear.

The force-displacement relationship of the mechanical system modeling the honeycomb in Fig. 2b can be found from the following equation

$$f = (k_2 + c_2 y)y + 6(k_1 + c_1 y)\cdot \cdot \left(\frac{\sqrt{h^2 + (\frac{L}{2})^2}}{\sqrt{(\frac{L}{2})^2 + (h-y)^2}} - 1 \right)(h - y) \tag{2}$$

where y is the vertical buckling displacement of the NSH, k_1 and k_2 are the linear stiffness characteristics of the springs, c_1 and c_2 are the nonlinear stiffness characteristics of the springs, f is the external force. The equation is similar to the one described in [48]–[50].

The proposed honeycomb structure consists of three identical double beams intersecting at 120° when viewed from the top, Fig. 2c-d. Double-curved beam configuration is used to transfer from the first-mode-buckled shape to the third-mode-buckled shape bypassing the second mode. The horizontal length of each beam was chosen as $L = 73.6$ mm, while depth $p = 5.00$ mm. Based on analytical modeling of Algorithm 1 from [12], the thickness of each beam was found as $t = 0.85$ mm, and the height of the middle point of the beam $h = 3.0$ mm. Three sets of double beams may be interpreted as columns i.e. number of columns $Z_c = 3$, number of rows $Z_r = 1$. These values of the parameters were selected to achieve a randomly chosen $f_{max} = 5$ N maximum load for a single beam configuration. Since there are 3 columns and double beams in each column, the overall force threshold for the whole sensor is six times larger ($f_{max} = 30$ N).

IV. End-Effector Design

The design of the experimental setup with an active negative stiffness honeycomb as an end-effector is shown in Fig. 3. The setup consists of the NSH structure, a robot manipulator (Universal Robot 5), a microcontroller (Teensy 3.6), a motor (Dynamixel MX-106), a Hall-effect sensor (Hall Effect Sensor Single Axis 8-SOIC 505-AD22151YRZ-ND, Analog Devices), a fishing line as a tendon, and guiding and holding structures. The detailed view of the proposed end-effector design can be seen in Fig. 4. The parts of the proposed honeycomb were printed by using the Ultimaker S5 with CPE (co-polyester) material. This mechanism is similar to the interlocking of Lego pieces, where the protrusions on one piece fit into the corresponding recesses on another, forming a cohesive and stable structure as shown in Fig. 2d. Such an approach helps to prevent a staircase effect in a curvilinear path occurring in planar layer-by-layer printing [51]. Various materials were tested on bucklings such as Nylon, PLA, Tough PLA, TPU 95A, and CPE. Ultimaker CPE (co-polyester) demonstrated the best behavior with distinguishable buckling and high endurance. Due to the chosen geometry of the

proposed honeycomb structure, during axial loading, the honeycomb beams move to the elastic negative stiffness instability phase. The proposed honeycomb structure was developed such that it has a metastable configuration, e.g. if the external load is removed, the honeycomb returns to its initial stable form.

One cylindrical neodymium magnet (with a length of 2.4 mm and a diameter of 6 mm) is connected to a 3D-printed support mechanism such that when the honeycomb buckles, the magnet also moves along the axis to the same distance as the center of the honeycomb structure. The Hall-effect sensor is located under the magnet and can sense the magnetic field intensity. To get unidirectional motion, a tendon passes through a linear bearing and a 3D-printed shaft which is fixed to the NSH with one end. A motor with a pulley (17mm diameter) can stretch the honeycomb vertically by 6.5 mm using the tendon.

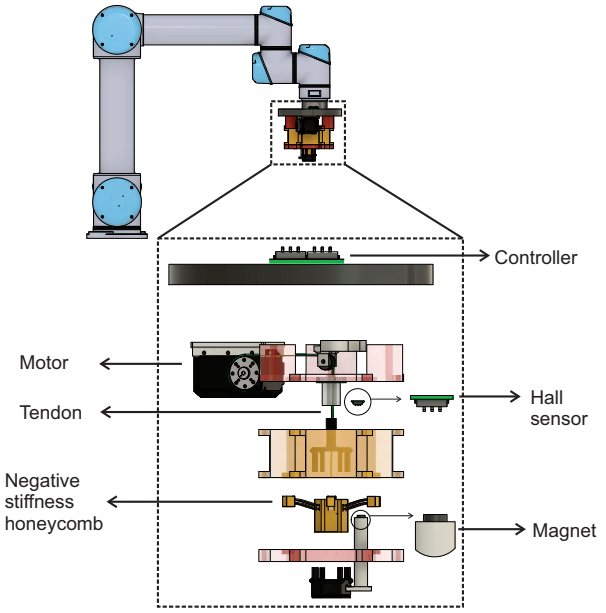

Fig. 3: Experimental setup: robot arm (UR5) with an exploded view of the attached active tactile sensor. The sensor consists of a 3D-printed negative stiffness honeycomb, Hall-effect sensor, neodymium magnet, microcontroller board, servo-motor (Dynamixel MX-106), tendon (spectra tendon), a pulley, a linear bearing, and guiding 3d-printed parts. The servo-motor controls the displacement of honeycomb beams by adjusting the tendon's tension. A Hall sensor measures the distance to the magnet, which is proportional to the beam's displacement.

A. Displacement based on Hall-effect sensor

The intensity of the magnetic field was measured by the Hall-effect sensor and converted to an analog signal by built-in Teensy's 10-bit ADC at a 500 Hz sampling rate. The magnetic field sensor was preliminarily calibrated by measuring its output data variation with the distance from the magnet to the Hall-effect sensor. A distance was measured by a digital caliper and a two-term exponential model was fitted to the experimental sensor output-distance data (Fig. 5).

Fig. 6 represents the force-displacement relationship of the proposed honeycomb structure received by conducting quasi-static tests. To measure the force exerted by the honeycomb during compression, we used a 6-axis Force/Torque sensor (WITTENSTEIN SE hex21 F/T sensor) in our experiments.

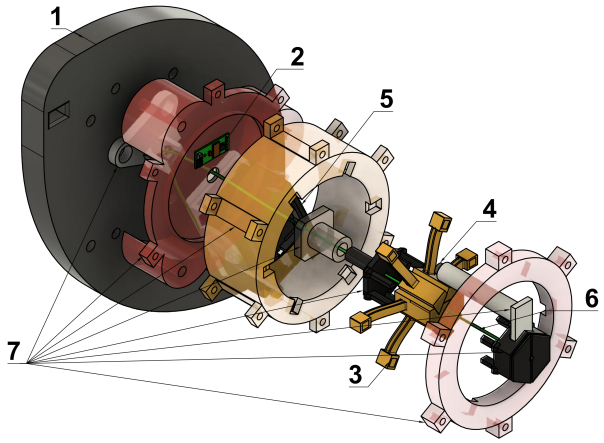

Fig. 4: Detailed view of the reconfigurable tactile sensor with variable stiffness: 1 - base, 2 - Hall Effect Sensor, 3 - proposed honeycomb structure, 4 - circular neodymium magnet, 5 - servomotor, 6 - tendon, 7 - guiding and holding structure (mounts).

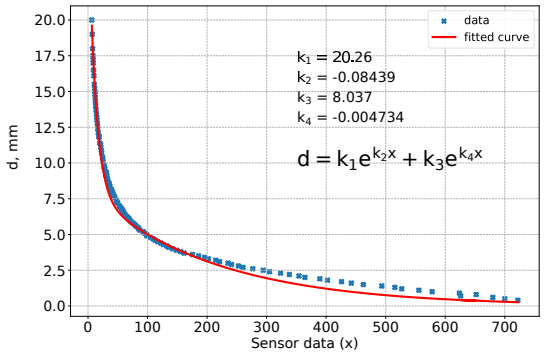

Fig. 5: Calibration results of the Hall effect sensor readings versus the beam's displacement. The raw ADC data from the analog Hall sensor is on the x-axis, and the beam displacement is on the y-axis. Then, the negative stiffness honeycomb displacement is approximated from the Hall-effect sensor readings by fitting the curve. The axes are rotated to show that the graph is used as a lookup table to find the estimates of the sensor deformation. Every sample is an average of multiple trials to improve the accuracy.

In the test, the robot arm with the proposed end-effector moved toward the F/T sensor at a speed of 90 mm/sec. This continued until the honeycomb reached the second positive stiffness zone. The displayed red curve represents an average derived from 10 trials (grey curves). The theoretical curve was received analytically using the method developed by [12]. The difference between theoretical and experimental curves could be due to the visco-elastic behavior of CPE material, potential moderate plastic deformation, or deformations in joints as explained in [15]. To consider the curve (Fig. 6, blue circles) received by the mechanical model from Fig. 2b, we assumed that oblique and vertical springs have only first-order nonlinearity. An optimization algorithm (L-BFGS-B) was applied to find the values of the coefficients used in (2): $k_1 = 100.0$ N/mm, $k_2 = 6.13$ N/mm, $c_1 = c_2 = 0.01$ N/mm^2, $h = 4.15$ mm, $L/2 = 19.56$ mm.

V. Experiments and Results

In this section, we present the results obtained from the experiments conducted to measure the dynamic properties of

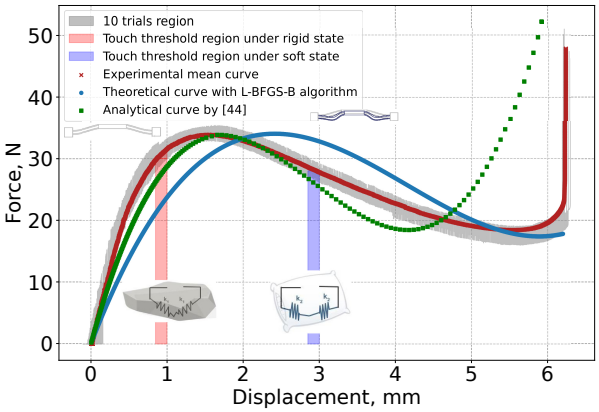

Fig. 6: Force-displacement characteristic of NSH sensor. Experimental Data samples include quasi-static tests conducted ten times (grey region) with a mean force-displacement curve (red cross), analytical results (green squares) for the model given by [12], analytical results (blue circles) for the model given by Equation 2. Touch threshold regions highlighted in pink and purple are used for Experiment I (Contact detection).

the NSH structures. These experiments would also confirm the safety and other functionalities of the proposed honeycomb structure when used in the robot for interaction with the environment. Firstly, we conducted contact detection experiments since it is a crucial safety function of robot manipulators. To this end, the impact force during contact was recorded. Secondly, experiments were performed to measure the energy storage and release capabilities of the honeycomb structures. This is achieved by altering the stiffness of the honeycomb sensor during a collision to vary dissipation levels and amplify impact energy.

The NSH sensor, "ground truth" F/T sensor, and robot arm were connected to a central PC (Z4 HP workstation with 32 GB DDR4, Intel Core i9, NVIDIA RTX2080Ti, and Linux operating system patched with the real-time kernel) running Robot Operating System (ROS), which received the data and saved it to a local data storage.

A. EXPERIMENT 1: Contact detection

In this experiment, the industrial robot manipulator UR5 with the proposed NSH structure as an end-effector moved horizontally until it collided with the fixed rigid wall containing the F/T sensor. During the collision, the F/T sensor measured the contact orce. The contact detection algorithm is based on measuring the displacement threshold of NSH during the collision. The Hall-effect sensor measures the displacement of NSH via the magnet attached to the buckling part of NSH. In the first part of the experiment, the NSH structure is initially (before the collision) precompressed to 0.85 mm (a rigid state in Fig. 6) by the tendon connected to the Dynamixel motor. During the collision, the manipulator was programmed to stop when the NSH buckling reached the displacement threshold of 0.15 mm (from 0.85 mm to 1.00 mm). The second part of the experiment is similar to the first part, except that the NSH is initially precompressed to 2.85 mm (a soft state in Fig. 6) by the tendon and the motor. The NSH structure should be additionally compressed by the same 0.15 mm threshold (from 2.85 mm to 3.00 mm) during the collision before the robot motion stops. Such procedure was conducted ten times for each state (rigid and soft), and mean impact force was calculated (red line in Fig. 7). It is seen that the impact force in the soft state is less than in the rigid state due to the lower stiffness zone (Fig. 7 b).

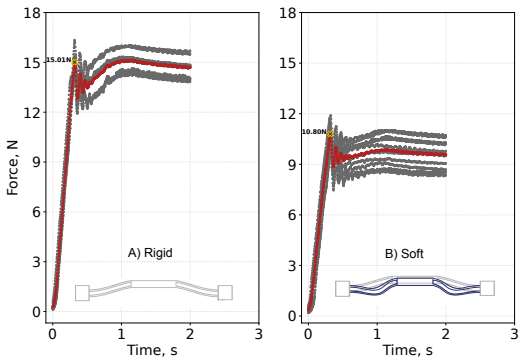

Fig. 7: Modifying impact force of NSH sensor for the contact detection under a) the rigid state and b) soft state. The maximum amplitude of 15 N in the rigid state is reduced to 11 N in the soft state, allowing lighter contact detection.

B. EXPERIMENT 2: Collision energy assessment using pendulum

In this experiment, by using a physical pendulum, we demonstrate the ability of the proposed NSH with reconfigurable stiffness to alter the collision energy. The experimental setup is illustrated in Fig. 8. A robot manipulator with an NSH end-effector collides at a set speed ($v_a = 30$ mm/sec) with the physical pendulum, made of a wooden block rigidly attached to an aluminum rod. The wooden block has a mass $m_p = 1.78$ kg, length $S_a = 12.4$ cm, width $S_b = 4.9$ cm, height $S_c = 12$ cm, and estimated moment of inertia around its center of mass $I_p = 0.32$ kg·m^2. At the same time, an aluminum hollow rod has a diameter of $r = 12.1$ mm, a mass of $m_r = 51$ g, and a length of $L_r = 36$ cm. For a clear momentum/energy transfer illustration, the rotation axis of the pendulum is fixed in the plane perpendicular to the impact force by attaching the pendulum's rod to a shaft with two bearings (each with a diameter of 2 mm) such that it has only 1 DOF (rotates around the shaft only). To record the impact acceleration resulting from the collision in different honeycomb configurations, the Sunfounder ADXL345 3-Axis Acceleration has been attached to the wooden cube and connected to the Teensy 3.6 Development Board, which collects the data from the accelerometer with a 500 Hz sampling rate. Such a low sampling rate does not allow us to reconstruct the collision event accurately and calculate the transferred energy. However, it enables estimating the maximum acceleration values, which can be used further to evaluate the collision energy differences. Each part of the experiment was conducted ten times, and the box plot of the peak accelerations is shown in Fig. 9 (on the right) with the corresponding angle of rotation of the pendulum on photos (on the left).

As in the previous experiments, we start with the first configuration, where the robot manipulator with the proposed

end-effector hits the pendulum when the honeycomb structure is not compressed (shown in Fig. 8 as a green case 3). Since the honeycomb is rigid, it has high stiffness and low damping, behaving as a rigid body. Therefore, as expected, it transmits most of the collision energy to the pendulum, which results in the amplitude of oscillations (maximum rotational angle) $\alpha_p \approx 2.4^\circ$ after the impact and the peak specific acceleration (expressed in g) $a_p \approx 0.73$ (second-row inset of Fig. 9).

Next, we modify the stiffness of the NSH structure to the soft state by compressing it by 3 mm with the tendon attached to the Dynamixel motor. Then, the end-effector collides with the pendulum at the same speed v_a. Since the honeycomb is soft, it demonstrates lower stiffness and higher damping than in the previous case. It also means that more kinetic energy from the robot arm is dissipated, reducing the contact force and the momentum transmitted to the pendulum. Hence, the pendulum has smaller rotational angle amplitude $\alpha_p \approx 1.8^\circ$ and the peak specific acceleration $a_p \approx 0.63$ (first-row inset of Fig. 9).

Finally, we test the dynamic case, where the NSH attached to the end-effector is in the precompressed state, and the tendon is released just before the collision. During this transition, the stiffness of the honeycomb increases. Therefore, the NSH structure releases the mechanical energy stored in its beams, transferring extra momentum to the pendulum. Thus, the transmitted energy includes the energy from the robot's motion and the energy released from the honeycomb. As a result, the pendulum experiences higher rotational angle amplitude $\alpha_p \approx 4.1^\circ$ and the peak specific acceleration $a_p \approx 0.87$ (see the third-row inset in Fig. 9). The experiments are similar to what was done by [52], and the results show the same pattern.

VI. Discussions

To demonstrate that the increased energy of the pendulum in the last experiment comes from the energy stored in the honeycomb, we compare the work done by the NSH structure W_{NSH} with the additional potential energy of the pendulum in the dynamic case ΔU. The work done by the NSH is evaluated as

$$W_{NSH} = \int_{y_i}^{y_f} F(y)dy, \tag{3}$$

where y_i and y_f are the initial and final buckling displacements of the NSH honeycomb, respectively. This integral can be found numerically by finding the area under the experimental curve of the force-displacement relationship (shown in Fig. 6)). In our case, $y_i = 0$ and $y_f = y_{max}$, where y_{max} is the displacement corresponding to the local maximum in the force-displacement graph. Once the NSH displacement reaches y_{max}, the honeycomb suddenly snaps into its second state. In other words, no external force is required to move the honeycomb after the displacement y_{max}. Using the experimental force-displacement curve, we estimate that $W_{NSH} = 36.1$ mJ using the experimental force-displacement curve.

The potential energy of the pendulum at the angle θ can be calculated as

$$U = m_p g(L_r + \frac{S_c}{2})(1 - \cos(\theta)). \tag{4}$$

The potential energies of the pendulum at the maximum angular displacement for the dynamic U_{dyn} and rigid cases U_{rig} are found by substituting $\theta = \alpha_p$ in the above equation. To see the increase in potential energy of the pendulum, the difference between the potential energies is evaluated as $\Delta U = U_{dyn} - U_{rig} = 17.9mJ - 6.6mJ = 11.3mJ$.

The efficiency of the honeycomb structure to store and release the potential energy can be evaluated as

$$\nu = \frac{\Delta U}{W_{NSH}}. \tag{5}$$

From the performed experiments, we estimate that $\nu \approx 0.31$. Thus, the efficiency of the honeycomb structure with the given material is around 30%. As the honeycomb is not perfectly elastic, some energy is lost due to dissipative forces, friction, and plastic deformation. The described dynamic state of NSH can be utilized to store, amplify, and release mechanical energy similar to muscles. This would enable rapid and explosive dynamic moions. For example, Wang et al. [53] used the concept of stored elastic potential energy for jumping robots.

Improved control of variable stiffness has several potential applications. By adjusting the stiffness to the optimal level at the moment of impact, the variable stiffness system can deliver powerful and precise impact for hammering tasks [54]. Also, it might be utilized to reduce the impact force to prevent or minimize the damage to the target or the actuator itself. When moving at high speeds, decreasing the stiffness ensures safe interaction and minimizes potential damage [55], [56] due to unexpected collision. While in a static configuration, stiffness can be increased for precise positioning and elastic behavior. Moreover, changing the stiffness during interaction can provide responsive haptic feedback to simulate impact sensation [57], [58].

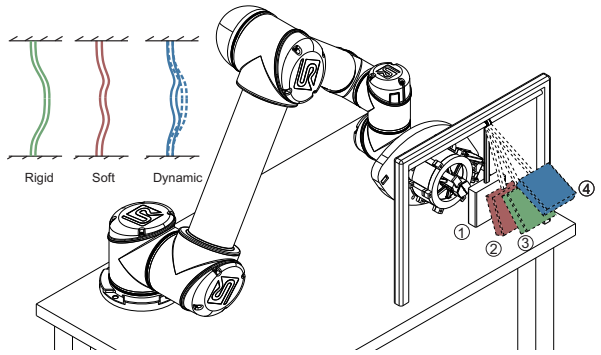

Fig. 8: Pendulum experiment concept: 1. Initial position, 2. inclination due to the push with compressed state of honeycomb, 3. inclination due to the push with rest state of honeycomb, 4. inclination due to the extra momentum

VII. Conclusions

This paper explored the capabilities of the honeycomb structures for contact detection, stiffness variation, and mechanical energy storage and release. Due to the nonlinear force-displacement characteristics, the honeycomb structures possess variable and negative stiffness behavior. The advantages of the negative stiffness behavior can be exploited by controlling the compression of the honeycomb. We demonstrated that the honeycomb can vary the contact stiffness of the end-effector during interaction with an external object. This, in

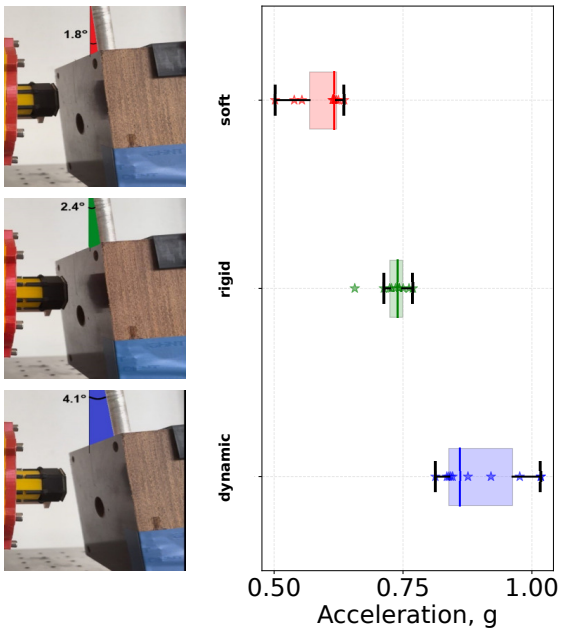

Fig. 9: Mean acceleration of the pendulum for three experimental cases: red - soft state, green - rigid state, blue - dynamic state. The inclination angle is proportional to the impact force and increases from 1.8° in the soft state to 4.1° in the dynamic state, demonstrating higher collision energy transfer.

turn, enabled soft and hard types of contact, which can be beneficial for applications related to soft robotics and robots with variable impedance joints. The tendon, controlled by an actuator, was utilized to precompress the honeycomb to the desired level. Additionally, the honeycomb structures containing a magnet and a Hall effect sensor enabled the detection of the contact event.

Furthermore, the honeycomb structures' energy storage and release capabilities were explored. The results demonstrate that the honeycomb structures can store the potential energy and then release it when desired. This enables them to function as muscles, opening the possibilities for the honeycomb structures to be utilized for dynamic and explosive tasks. Our sensor may be used not only as a collision detection mechanism but also for manipulation with different stiffness levels and for getting appropriate dynamic responses without tuning the internal parameters of the manipulator or the controller. The paper presents and summarizes the results of the extensive experimental work.

Variable stiffness metamaterial structures can also potentially be used for points-based shape recognition (soft state). Compliance is the critical factor for robustness during interaction and safety for the environment and robot. Compliant materials can provide benefits such as improved adaptability, enhanced force control, increased energy efficiency, and protection against damage in case of collisions or unexpected loads. Variable stiffness metamaterial structures based on curved beams are compliant and can be applied for grasping. During grasping, the negative stiffness component can help mitigate excessive grasping forces and enhance the sensitivity in interacting with delicate objects.

The developed contact detection is limited to a single point. Extending the honeycomb structure to an array of sensors to develop tactile skin is possible. Moreover, the NSH could be replaced by a compliant system with near-zero stiffness to increase stable control and improve the gripping capabilities of robot end-effectors that handle delicate, soft, rigid, and complex-shaped objects. Designing and incorporating the properties of new metamaterials with exotic mechanical properties composed of bistable and metastable honeycomb structures will potentially enhance the state-of-the-art tactile sensors.

Acknowledgments

The authors are thankful to Temirlan Galimzhanov and Atakan Varol for the discussions on the structure of the sensor.

References

[1] M. Selvaggio, M. Cognetti, S. Nikolaidis, S. Ivaldi, and B. Siciliano, "Autonomy in physical human-robot interaction: A brief survey," *IEEE Robotics and Automation Letters*, vol. 6, no. 4, pp. 7989–7996, 2021.

[2] S. Haddadin, A. De Luca, and A. Albu-Schäffer, "Robot collisions: A survey on detection, isolation, and identification," *IEEE Transactions on Robotics*, vol. 33, no. 6, pp. 1292–1312, 2017.

[3] V. Padois, S. Ivaldi, J. Babič, M. Mistry, J. Peters, and F. Nori, "Whole-body multi-contact motion in humans and humanoids: Advances of the codyco european project," *Robotics and Autonomous Systems*, vol. 90, pp. 97–117, 2017, special Issue on New Research Frontiers for Intelligent Autonomous Systems.

[4] L. Righetti, M. Kalakrishnan, P. Pastor, J. Binney, J. Kelly, R. C. Voorhies, G. S. Sukhatme, and S. Schaal, "An autonomous manipulation system based on force control and optimization," *Autonomous Robots*, vol. 36, pp. 11–30, 2014.

[5] Q. Li, O. Kroemer, Z. Su, F. F. Veiga, M. Kaboli, and H. J. Ritter, "A review of tactile information: Perception and action through touch," *IEEE Transactions on Robotics*, vol. 36, no. 6, pp. 1619–1634, 2020.

[6] R. Dahiya, N. Yogeswaran, F. Liu, L. Manjakkal, E. Burdet, V. Hayward, and H. Jörntell, "Large-area soft e-skin: The challenges beyond sensor designs," *Proceedings of the IEEE*, vol. 107, no. 10, pp. 2016–2033, 2019.

[7] N. F. Lepora, "Soft biomimetic optical tactile sensing with the tactip: A review," *IEEE Sensors Journal*, vol. 21, no. 19, pp. 21 131–21 143, 2021.

[8] P. Mittendorfer and G. Cheng, "Humanoid multimodal tactile-sensing modules," *IEEE Transactions on Robotics*, vol. 27, no. 3, pp. 401–410, 2011.

[9] T. Galimzhanov, A. Zhakatayev, R. Kashapov, Z. Kappassov, and H. A. Varol, "Linear negative stiffness honeycomb actuator with integrated force sensing," in *2020 IEEE/ASME International Conference on Advanced Intelligent Mechatronics (AIM)*, 2020, pp. 1589–1594.

[10] G. Anderson, "Stability of a manipulator with resilient joints," *Journal of Sound and Vibration*, vol. 101, no. 4, pp. 463–480, 1985.

[11] A. Rosales and T. Heikkilä, "Analysis and design of direct force control for robots in contact with uneven surfaces," *Applied Sciences*, vol. 13, no. 12, 2023.

[12] A. Zhakatayev, Z. Kappassov, and H. A. Varol, "Analytical modeling and design of negative stiffness honeycombs," *Smart Materials and Structures*, vol. 29, no. 4, 2020.

[13] E. Barchiesi, M. Spagnuolo, and L. Placidi, "Mechanical metamaterials: a state of the art," *Mathematics and Mechanics of Solids*, vol. 24, no. 1, pp. 212–234, 2019.

[14] C. Guo, D. Zhao, Z. Liu, Q. Ding, H. Gao, Q. Yan, Y. Sun, and F. Ren, "The 3D-printed honeycomb metamaterials tubes with tunable negative Poisson's Ratio for high-performance static and dynamic mechanical properties," *Materials*, vol. 14, no. 6, p. 1353, 2021.

[15] D. M. Correa, T. Klatt, S. Cortes, M. Haberman, D. Kovar, and C. Seepersad, "Negative stiffness honeycombs for recoverable shock isolation," *Rapid Prototyping Journal*, 2015.

[16] H. Nguyen, R. Fangueiro, F. Ferreira, and Q. Nguyen, "Auxetic materials and structures for potential defense applications: An overview and recent developments," *Textile Research Journal*, vol. 93, no. 23-24, pp. 5268–5306, 2023.

[17] E. T. Filipov, T. Tachi, and G. H. Paulino, "Origami tubes assembled into stiff, yet reconfigurable structures and metamaterials," *Proceedings of the National Academy of Sciences*, vol. 112, no. 40, pp. 12 321–12 326, 2015.

[18] S. Barbarino, F. S. Gandhi, and R. Visdeloup, "A bi-stable von-mises truss for morphing applications actuated using shape memory alloys," in *Smart Materials, Adaptive Structures and Intelligent Systems*, vol. 56031. American Society of Mechanical Engineers, 2013, p. V001T01A004.

[19] H. Du, F. S. Chau, and G. Zhou, "Harmonically-driven snapping of a micromachined bistable mechanism with ultra-small actuation stroke," *Journal of Microelectromechanical Systems*, vol. 27, no. 1, pp. 34–39, 2018.

[20] T. Mei, Z. Meng, K. Zhao, and C. Q. Chen, "A mechanical metamaterial with reprogrammable logical functions," *Nature communications*, vol. 12, no. 1, p. 7234, 2021.

[21] S. Haddadin, A. Albu-Schaffer, A. De Luca, and G. Hirzinger, "Collision detection and reaction: A contribution to safe physical human-robot interaction," in *2008 IEEE/RSJ International Conference on Intelligent Robots and Systems*. IEEE, 2008, pp. 3356–3363.

[22] A. De Luca and R. Mattone, "Sensorless robot collision detection and hybrid force/motion control," in *Proceedings of the 2005 IEEE international conference on robotics and automation*. IEEE, 2005, pp. 999–1004.

[23] G. Garofalo, N. Mansfeld, J. Jankowski, and C. Ott, "Sliding mode momentum observers for estimation of external torques and joint acceleration," in *2019 International Conference on Robotics and Automation (ICRA)*. IEEE, 2019, pp. 6117–6123.

[24] A. De Luca, A. Albu-Schaffer, S. Haddadin, and G. Hirzinger, "Collision detection and safe reaction with the DLR-III lightweight manipulator arm," in *2006 IEEE/RSJ International Conference on Intelligent Robots and Systems*. IEEE, 2006, pp. 1623–1630.

[25] S. Mamedov and S. Mikhel, "Practical aspects of model-based collision detection," *Frontiers in Robotics and AI*, vol. 7, p. 571574, 2020.

[26] W.-H. Chen, D. J. Ballance, P. J. Gawthrop, and J. O'Reilly, "A nonlinear disturbance observer for robotic manipulators," *IEEE Transactions on industrial Electronics*, vol. 47, no. 4, pp. 932–938, 2000.

[27] J. Hu and R. Xiong, "Contact force estimation for robot manipulator using semiparametric model and disturbance Kalman filter," *IEEE Transactions on Industrial Electronics*, vol. 65, no. 4, pp. 3365–3375, 2017.

[28] M. Van Damme, P. Beyl, B. Vanderborght, V. Grosu, R. Van Ham, I. Vanderniepen, A. Matthys, and D. Lefeber, "Estimating robot end-effector force from noisy actuator torque measurements," in *2011 IEEE International Conference on Robotics and Automation*. IEEE, 2011, pp. 1108–1113.

[29] J. van Dam, A. Tulbure, M. V. Minniti, F. Abi-Farraj, and M. Hutter, "Collision detection and identification for a legged manipulator," *arXiv preprint arXiv:2207.14745*, 2022.

[30] P. Cao, Y. Gan, and X. Dai, "Model-based sensorless robot collision detection under model uncertainties with a fast dynamics identification," *International Journal of Advanced Robotic Systems*, vol. 16, no. 3, p. 1729881419853713, 2019.

[31] R. S. Dahiya, G. Metta, M. Valle, and G. Sandini, "Tactile sensing—from humans to humanoids," *IEEE transactions on robotics*, vol. 26, no. 1, pp. 1–20, 2009.

[32] R. Patel, R. Cox, and N. Correll, "Integrated proximity, contact and force sensing using elastomer-embedded commodity proximity sensors," *Autonomous Robots*, vol. 42, pp. 1443–1458, 2018.

[33] P. Mittendorfer and G. Cheng, "Humanoid multimodal tactile-sensing modules," *IEEE Transactions on robotics*, vol. 27, no. 3, pp. 401–410, 2011.

[34] D. Sandykbayeva, Z. Kappassov, and B. Orazbayev, "Vibrotouch: Active tactile sensor for contact detection and force sensing via vibrations," *Sensors*, vol. 22, no. 17, p. 6456, 2022.

[35] M. Kaboli and G. Cheng, "Robust tactile descriptors for discriminating objects from textural properties via artificial robotic skin," *IEEE Transactions on Robotics*, vol. 34, no. 4, pp. 985–1003, 2018.

[36] K. M. Park, J. Kim, J. Park, and F. C. Park, "Learning-based real-time detection of robot collisions without joint torque sensors," *IEEE Robotics and Automation letters*, vol. 6, no. 1, pp. 103–110, 2020.

[37] A.-N. Sharkawy, P. N. Koustoumpardis, and N. Aspragathos, "Human–robot collisions detection for safe human–robot interaction using one multi-input–output neural network," *Soft Computing*, vol. 24, pp. 6687–6719, 2020.

[38] K. M. Park, Y. Park, S. Yoon, and F. C. Park, "Collision detection for robot manipulators using unsupervised anomaly detection algorithms," *IEEE/ASME Transactions on Mechatronics*, vol. 27, no. 5, pp. 2841–2851, 2021.

[39] D. Kim, D. Lim, and J. Park, "Transferable collision detection learning for collaborative manipulator using versatile modularized neural network," *IEEE Transactions on Robotics*, vol. 38, no. 4, pp. 2426–2445, 2021.

[40] S. Chen, X. Tan, J. Hu, S. Zhu, B. Wang, L. Wang, Y. Jin, and L. Wu, "A novel gradient negative stiffness honeycomb for recoverable energy absorption," *Composites Part B: Engineering*, vol. 215, p. 108745, 2021.

[41] O. A. Ganilova and J. J. Low, "Application of smart honeycomb structures for automotive passive safety," *Proceedings of the Institution of Mechanical Engineers, Part D: Journal of Automobile Engineering*, vol. 232, no. 6, pp. 797–811, 2018.

[42] D. A. Debeau, C. C. Seepersad, and M. R. Haberman, "Impact behavior of negative stiffness honeycomb materials," *Journal of Materials Research*, vol. 33, no. 3, pp. 290–299, 2018.

[43] C. Ren, D. Yang, and H. Qin, "Mechanical performance of multidirectional buckling-based negative stiffness metamaterials: an analytical and numerical study," *Materials*, vol. 11, no. 7, p. 1078, 2018.

[44] X. Tan, B. Wang, S. Zhu, S. Chen, K. Yao, P. Xu, L. Wu, and Y. Sun, "Novel multidirectional negative stiffness mechanical metamaterials," *Smart Materials and Structures*, vol. 29, no. 1, p. 015037, 2019.

[45] Z. Meng, W. Chen, T. Mei, Y. Lai, Y. Li, and C. Chen, "Bistability-based foldable origami mechanical logic gates," *Extreme Mechanics Letters*, vol. 43, p. 101180, 2021.

[46] H. Yang, N. D'Ambrosio, P. Liu, D. Pasini, and L. Ma, "Shape memory mechanical metamaterials," *Materials Today*, vol. 66, pp. 36–49, 2023.

[47] J. Qiu, J. H. Lang, and A. H. Slocum, "A curved-beam bistable mechanism," *Journal of microelectromechanical systems*, vol. 13, no. 2, pp. 137–146, 2004.

[48] H. Li, Y. Li, and J. Li, "Negative stiffness devices for vibration isolation applications: a review," *Advances in Structural Engineering*, vol. 23, no. 8, pp. 1739–1755, 2020.

[49] S. Dalela, P. Balaji, and D. Jena, "Design of a metastructure for vibration isolation with quasi-zero-stiffness characteristics using bistable curved beam," *Nonlinear Dynamics*, vol. 108, no. 3, pp. 1931–1971, 2022.

[50] C.-C. Lan, S.-A. Yang, and Y.-S. Wu, "Design and experiment of a compact quasi-zero-stiffness isolator capable of a wide range of loads," *Journal of Sound and Vibration*, vol. 333, no. 20, pp. 4843–4858, 2014.

[51] W. Oropallo and L. A. Piegl, "Ten challenges in 3D printing," *Engineering with Computers*, vol. 32, pp. 135–148, 2016.

[52] H. Jin, M. Luo, S. Lu, Q. He, and Y. Lin, "Design and analysis of a novel variable stiffness joint for robot," in *Actuators*, vol. 12, no. 1. MDPI, 2022, p. 10.

[53] Y. Wang, Q. Wang, M. Liu, Y. Qin, L. Cheng, O. Bolmin, M. Alleyne, A. Wissa, R. H. Baughman, D. Vella, *et al.*, "Insect-scale jumping robots enabled by a dynamic buckling cascade," *Proceedings of the National Academy of Sciences*, vol. 120, no. 5, p. e2210651120, 2023.

[54] M. Garabini, A. Passaglia, F. Belo, P. Salaris, and A. Bicchi, "Optimality principles in variable stiffness control: The vsa hammer," in *2011 IEEE/RSJ International Conference on Intelligent Robots and Systems*. IEEE, 2011, pp. 3770–3775.

[55] A. Bicchi and G. Tonietti, "Fast and" soft-arm" tactics [robot arm design]," *IEEE Robotics & Automation Magazine*, vol. 11, no. 2, pp. 22–33, 2004.

[56] G. Gasparri, M. Garabini, L. Pallottino, L. Malagia, M. Catalano, G. Grioli, and A. Bicchi, "Variable stiffness control for oscillation damping," in *2015 IEEE/RSJ International Conference on Intelligent Robots and Systems (IROS)*. IEEE, 2015, pp. 6543–6550.

[57] B. C. Mac Murray, B. N. Peele, P. Xu, J. Spjut, O. Shapira, D. Luebke, and R. F. Shepherd, "A variable shape and variable stiffness controller for haptic virtual interactions," in *2018 IEEE International Conference on Soft Robotics (RoboSoft)*. IEEE, 2018, pp. 264–269.

[58] F. Zuliani and J. Paik, "Variable stiffness folding joints for haptic feedback," in *2021 IEEE/RSJ International Conference on Intelligent Robots and Systems (IROS)*. IEEE, 2021, pp. 8332–8338.

Rustam Chibar received the Bachelor's and Master's degrees in robotics from the Nazarbayev University, Astana, Kazakhstan, in 2021 and 2023, respectively. He is currently a Senior Research Assistant at Tactile Robotics Lab, Nazarbayev University. His research interests include mechanical metamaterials, tactile sensing, human-robot interaction.

Valeriya Kostyukova received the B.Sc. degree in Robotics and Mechatronics, Nazarbayev University, Astana, Kazakhstan, in 2024. She s currently pursuing her M.Sc. degree and working as a research assistant at Tactile Robotics Laboratory. Her research interests include embedded systems design, signal processing, and microcontroller programming.

Soibkhon Khajikhanov received the B.Sc. degree in Robotics and Mechatronics, Nazarbayev University, Astana, Kazakhstan, in 2023. He is currently pursuing his M.Sc. degree and working as a Research Assistant in the Department of Robotics and Mechatronics at Nazarbayev University. His research interests is in the fields of tactile robotics and AR.

Daryn Kenzhebek received the B.Sc. degree in Robotics Engineering, Nazarbayev University, Astana, Kazakhstan, in 2024. He is currently pursuing his M.Sc. degree and working as a Research Assistant in the Department of Robotics and Mechatronics at Nazarbayev University. His research interests is in the fields of mechatronics.

Altay Zhakatayev (M'15) received his Ph.D. from the Robotics Department at Nazarbayev University in 2020. Previously, he worked as a postdoctoral researcher in the Information and Communication Technology Department at the University of Agder, Kristiansand, Norway. Before that, he worked as a research assistant at the Advanced Robotics and Mechatronics Systems (ARMS) Laboratory of Nazarbayev University, Astana, Kazakhstan. Currently, he is an Assistant Professor in the Mechanical and Aerospace Engineering Department at Nazarbayev University, Kazakhstan. His research interests include optimal control, analytical mechanics, state estimation, and nonlinear dynamics.

Bakhtiyar Orazbayev received a specialist diploma in Radio Physics from the People's Friendship University of Russia, Moscow, Russian Federation. After, he obtained M.S. and Ph.D. degrees from the Public University of Navarre (UPNA), Pamplona, Spain, in 2015 and 2016. Since 2021, he has been an assistant professor in the physics department at Nazarbayev University. His current research interests span a broad range of areas, including metamaterials, wave physics, and deep learning. He published 20 scientific articles in international journals (2 invited) during his research career. He has participated in 7 research projects and more than 30 international conferences. He also won several awards, including the UPNA Research Award in 2019 and the CST University Publication Award in 2016.

Zhanat Kappassov (Senior Member, IEEE) received the Specialist in Radio-engineering degree from the Tomsk State University of Control Systems and Radioelectronics, Russia. He worked in Industrial Technology Research Institute, Taiwan. He has obtained PhD in Robotics from Universite Pierre et Marie Curie, France. He is an Assistant Professor of Robotics Department, Nazarbayev University. He was a Postdoctoral Fellow at Bentley University, Boston, USA. His current research interests mainly focus on tactile sensing that involves robot physical interaction and dexterous manipulation. His PhD thesis was nominated as the Best PhD Thesis 2017 by the GDR Robotique association.